Optical Properties and Surface Enhanced Raman Scattering of L-Shaped Silver Nanorod Arrays

ARTICLE *in* THE JOURNAL OF PHYSICAL CHEMISTRY C · JULY 2011

Impact Factor: 4.77 · DOI: 10.1021/jp204389v

5 AUTHORS, INCLUDING:

Qin Zhou
Tsinghua University
23 PUBLICATIONS **338** CITATIONS
SEE PROFILE

Justin L Abell
University of Georgia
21 PUBLICATIONS **228** CITATIONS
SEE PROFILE

Zhengjun Zhang
Tsinghua University
191 PUBLICATIONS **2,715** CITATIONS
SEE PROFILE

THE JOURNAL OF PHYSICAL CHEMISTRY C

ARTICLE

pubs.acs.org/JPCC

Optical Properties and Surface Enhanced Raman Scattering of L-Shaped Silver Nanorod Arrays

Qin Zhou,[†,‡] Yuping He,[†] Justin Abell,[†] Zhengjun Zhang,[‡] and Yiping Zhao*[,†]

[†]Department of Physics and Astronomy, Nanoscale Science and Engineering Center, The University of Georgia, Athens, Georgia 30602, United States

[‡]Advanced Materials Laboratory, Department of Materials Science and Engineering, Tsinghua University, Beijing 100084, People's Republic of China

Supporting Information

ABSTRACT: Optical reflection, transmission, and surface-enhanced Raman scattering (SERS) of L-shaped silver nanorod arrays with different lengths prepared by oblique angle deposition are studied and compared in detail to those properties of straight silver nanorod arrays. With the increase of the arm length of both the L-shaped and straight nanorods, the optical reflectance increases, but the transmittance decreases. The reflectance of L-shaped Ag nanorods is similar to that of straight nanorods with the same total length, but the transmittance is lower for the former than for the latter. Transfer matrix method for multilayer thin films based on anisotropic effective medium theory has been used to calculate the optical properties of both the L-shaped and straight Ag nanorod arrays, and the calculated results are qualitatively consistent with the experimental results. The SERS enhancement of the L-shaped and straight Ag nanorod arrays increases when the total arm length increases from 350 to 650 nm. The SERS behavior can be interpreted qualitatively by the thickness dependence of the optical absorbance effect.

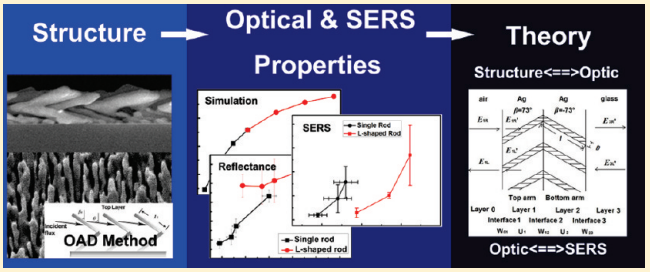

1. INTRODUCTION

Silver nanostructures have attracted considerable interest due to their significant surface-enhanced Raman scattering (SERS) property.[1−4] SERS is recognized as an ultrasensitive tool to detect low concentrations of molecules,[5−7] even to the single molecule level.[8,9] There are two main mechanisms that have been widely accepted for producing SERS: the electromagnetic (EM) mechanism and the chemical (CHEM) mechanism.[10,11] The EM mechanism, which is recognized as the major contributor, is due to the enhanced local electric field when the nanostructure is excited around its local surface plasmon resonance (LSPR) wavelength. The EM enhancement strongly depends on the shape, size, separation, arrangement of the particles, and dielectric environment around the particles.[12−14] The enormous enhancement of the Raman scattering is believed to originate from the surface locations with extremely high local electric field enhancement, which is generally called "hot spots". The "hot spots" are due to the specific nanoscale topologies of the surface of metal with large negative real part and small positive imaginary part of dielectric constant, such as Ag and Au.[9,14,15] Many theoretical calculations have demonstrated that if there are singularities in nanostructures, the local electric fields at those locations will be greatly enhanced, which give the hot spots.[16−19] They predict that the nanorods with complicated shapes, such as periodic, L, and Y shapes, have more hot spots than that of a perfectly cylindrical nanorod.[16,18,19] Thus, it is expected that one will observe stronger SERS signal or have more opportunity to observe SERS of a small amount of molecules on irregular nanorods such as L-shaped nanorods than on cylindrical nanorods. The L-shaped nanorods is the simplest structure to have corners.[16,18,19] However, it is very hard to use conventional nanorod fabrication techniques to produce L-shaped nanorods systematically. For example, electrochemical deposition,[20] porous anodic aluminum oxide (AAO) template method,[21] and electron beam lithography technique are all able to produce silver nanorods,[22] but none of them can be used or has been used to make nanorods with multiple corners.[20−22]

Recently, in our laboratories, we have used the oblique angle deposition (OAD) method to fabricate Ag nanorod arrays as sensitive SERS substrates.[19,23−29] OAD is a physical vapor deposition method that can produce nanostructured metal films by simply controlling the deposition angle and thickness. The main growth mechanism of OAD is the self-shadowing effect and surface adatoms diffusion effect. In addition, the topology of the nanorod resulting from OAD can be tuned through programming the substrate rotation by a computer, thus three-dimensional shapes such as spiral, zigzag, C, or beadlike shapes, or multilayered spiral/rod structures can be fabricated.[30−40] The silver nanorod arrays prepared by OAD have been demonstrated

Received: May 11, 2011
Revised: June 11, 2011
Published: June 20, 2011

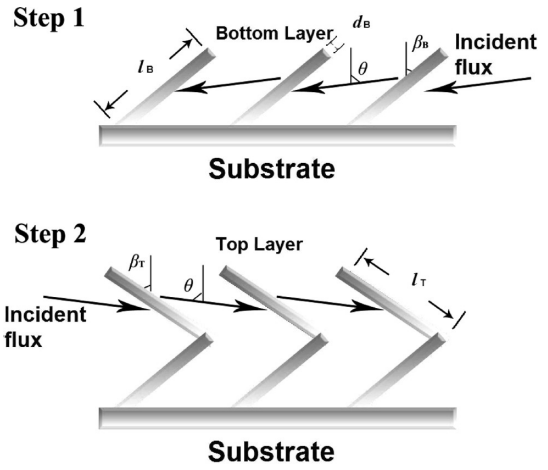

Figure 1. Depositing method to prepare L-shaped Ag nanorod arrays by OAD.

as very good SERS substrates, and they can be used to detect and differentiate viruses,[41−43] bacteria,[44] microRNA,[45,46] and sense trace amount of nuclear agents[47] and chemical molecules.[25,27,28,48] With substrate rotation, one can easily use OAD to fabricate metallic nanostructures with desired singularities like L-shaped nanorods which may have better SERS performance.

In this paper, we report our effort on fabricating L-shaped silver nanorod arrays systematically viathe OAD method and on the analysis of their optical and SERS properties. We have carried out UV−vis measurements and theoretic calculations on optical properties of L-shaped nanorods based on double-layer anisotropic effective medium theory and compared their optical properties with those from straight nanorods. The SERS properties of the L-shaped silver nanorod arrays and straight nanorod arrays have also been investigated and compared.

2. EXPERIMENTS

The L-shaped Ag nanorod arrays were fabricated by two consecutive OAD depositions using a custom-designed electron-beam evaporation system as shown in Figure 1. For the first deposition, the deposition flux was incident onto a flat glass substrate with an angle $\theta = 86°$ with respect to the surface normal of the substrate. After deposition for a fixed thickness, the substrate was rotated, and the flux was incident onto the substrate with an angle $-\theta$ to form the L shape (Figure 1). For the two consecutive OAD depositions, the thicknesses of Ag, monitored by a quartz crystal microbalance (QCM) positioned facing toward the vapor source, were the same. We fabricated different L-shaped Ag nanorod arrays with different QCM thickness readings: d_{QCM} = 1200, 1600, 2000, and 2400 nm, respectively, for each arm, in order to investigate how the optical property of L-shaped Ag nanorod film changes as a function of nanorod arm length. We also prepared straight Ag nanorod array samples under the same vapor incident angle with QCM thickness reading: d_{QCM} = 1200, 1600, 2000, and 2400 nm, as controls. The actual thickness and arm length of Ag nanorod arrays were different from the QCM reading due to the geometric shadowing effect and were determined by electron microscopy method. For nanorod fabrication, the background pressure in the chamber was 1×10^{-6} Torr, and the Ag deposition rate was 0.3 nm/s. Before deposition, the glass slide substrates were cleaned using piranha solution (H_2SO_4:H_2O_2 = 4:1). The source material for evaporation was Ag pellets (99.999%) purchased from the Kurt J. Lesker Company.

The morphologies of the obtained Ag nanorod arrays were characterized by a field-emission scanning electron microscope (SEM, FEI Inspect F). The optical properties of the L-shaped Ag nanorod arrays were measured by an UV−vis double beam spectrophotometer (Shimadzu UV−vis 2450).

Surface-enhanced Raman spectra (SERS) were measured by a HRC-10HT Raman analyzer from Enwave Optronics Inc., with a laser power of 30 ± 1 mW at the excitation wavelength of 785 nm and measuring time of 10 s. A 1 μL droplet of a Raman probe molecule, *trans*-1,2-bis(4-pyridyl)ethane (BPE, 10^{-5} M), was uniformly dispersed onto the Ag nanorod array substrates before the SERS measurements were carried out.

3. RESULTS AND DISCUSSION

3.1. Morphology Characterization of L-Shaped Nanorods. The representative top view and cross-section view SEM images of an L-shaped Ag nanorod array, with d_{QCM} = 1200 nm for each arm, are shown in Figure 2a. A clear bending between two arms as shown in the insert of Figure 2a demonstrates the success in L-shaped nanorod fabrication. When d_{QCM} = 1200 nm for each arm, the length of the bottom arm, $l_B = 360 \pm 40$ nm; the tilted angle of the bottom arm, β_B =70 ± 3° with respect to the substrate normal; the length of the top arm, $l_T = 390 \pm 50$ nm; and the tilted angle $\beta_T = 66 \pm 3°$. When d_{QCM} =1600 nm, $l_B = 560 \pm 90$ nm, $\beta_B = 73 \pm 4°$, $l_T = 520 \pm 50$ nm, and $\beta_T = 63 \pm 6°$, respectively. When d_{QCM} =2000 nm, $l_B = 640 \pm 60$ nm, $\beta_B = 73 \pm 2°$, $l_T = 650 \pm 60$ nm, and $\beta_T = 74 \pm 4°$, respectively. When the QCM reading is 2400 nm, the lengths of the bottom and top arm are 1200 ± 100 and 1070 ± 90 nm, respectively; the tilted angles of the bottom and top arms are 77 ± 2° and 75 ± 2°, respectively. The length and tilting angle of the each arm with different arm numbers are shown in Table 1. The bottom and top layer arm length and tilted angle versus QCM reading are shown in panels b and c of Figure 2, respectively. The arm length increases nearly linearly with the QCM reading, and the bottom layer tilted angle changes a little with QCM reading. The average bending angle between the two arms is about 40°. The top morphology of the L-shaped silver nanorod arrays remains unchanged when deposited with different arm lengths.

3.2. Optical Properties of L-Shaped Nanorods. Figure 3 shows the UV−vis reflectance and transmittance spectra of the L-shaped and single straight Ag nanorod arrays. For all the samples, the shapes of the spectra, either reflectance or transmittance, are quite similar; they all have a nearly constant reflectance R and transmittance T in the near-IR region, and the reflectance R deceases sharply when wavelength λ < 350 nm, and the transmittance T has a peak around λ = 320 nm. The reflectance of the L-shaped Ag nanorod arrays becomes larger and their transmittance becomes smaller when the arms of the L-shaped nanorods become longer. The reflectance and transmittance of the single Ag nanorod arrays follow the same trend as that of the L-shaped Ag nanorod arrays, but the reflectance is smaller than that of the L-shaped Ag nanorod arrays with the same bottom or top arm length, while the transmittance is larger than that of the L-shaped Ag nanorod arrays. Figure 4 shows the reflectance and transmittance at λ = 550 nm change as a function of the total length of the nanorods For the L-shaped nanorods, the total length is the sum of l_T and l_B, while for the single straight nanorods, the total length is the rod length . The total length of the L-shaped rods with two arms is approximately

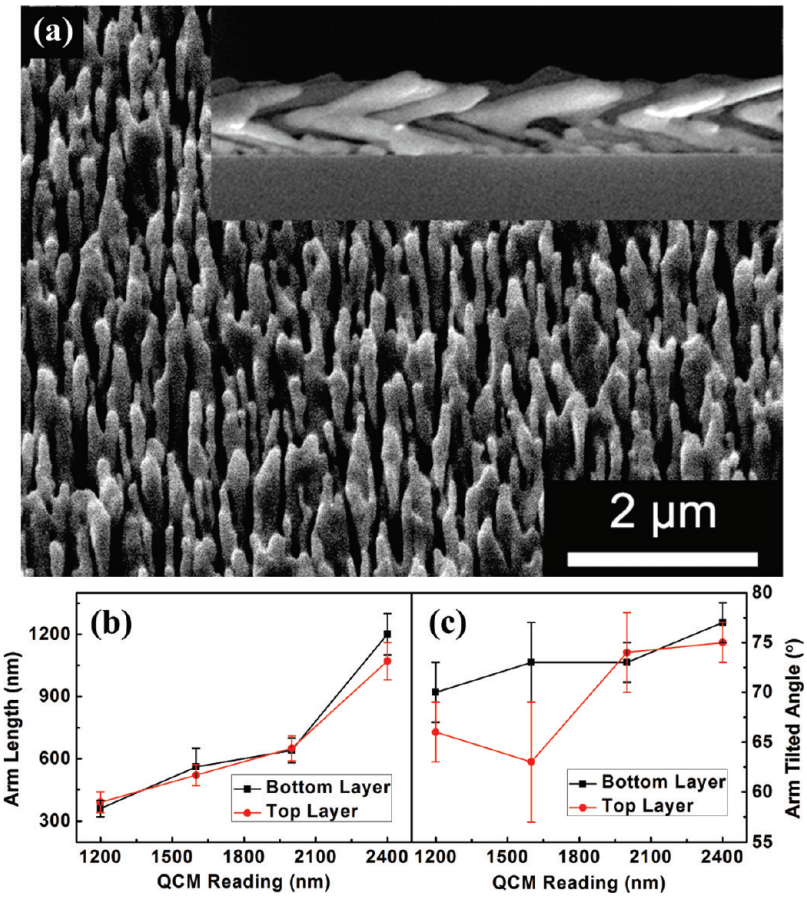

Figure 2. Morphology of L-shaped Ag nanorod arrays: (a) SEM image of L-shaped Ag nanorod arrays; (b) the bottom and top layer arm length vs QCM reading; (c) tilted angle vs QCM reading.

Table 1. Arm Length and Tilting Angle of L-Shaped Ag Nanorods with Different QCM Reading

QCM reading (nm)	top arm length (nm)	bottom arm length (nm)	top arm tilting angle (deg)	bottom arm tilting angle (deg)
1200	390 ± 50	360 ± 40	66 ± 3	70 ± 3
1600	520 ± 50	560 ± 90	63 ± 6	73 ± 4
2000	650 ± 60	640 ± 60	74 ± 4	73 ± 2
2400	1070 ± 90	1200 ± 100	75 ± 2	77 ± 2

twice that of the single nanorods with one arm. A general trend can be seen: with the increase of the total length, both the reflectance and transmittance change monotonically, that is, the R increases but the T decreases. The reflectance of the L-shaped nanorod arrays is similar to that of the single nanorod arrays with the same total length, while the transmittance of the L-shaped nanorod arrays is much lower to that of the single nanorod arrays with the same total length.

3.3. Calculated Optical Properties of Ag Nanorods. The L-shaped and straight Ag nanorods can be treated as a multilayer system, and the optical properties of both the L-shaped and straight Ag nanorods can be estimated by the effective medium theory. We used the N-layer matrix method and Fresnel formula to calculate reflectance and transmittance of this multilayer system.[49−54] The L-shaped nanorod layer can be treated as two anisotropic layers due to the tilting nature. We consider a four-layer model which is composed of an air layer (layer 0), top arm of the L-shaped nanorod layer (layer 1), bottom arm of L-shaped nanorod layer (layer 2), and glass layer (layer 3), as sketched in Figure 5. We define that the top Ag NR layer (layer 1) as an effective medium layer with a thickness d_T which is a mixture of air and the porous Ag nanorods tilted at an angle β_T with respect to surface normal, and the bottom Ag layer (layer 2) as another effective medium layer with a thickness of $d_B = d_T$ which is also a mixture of air and the porous nanorod array with a tilting angle of $\beta_B = -\beta_T$. To simplify, we assume that each Ag NR has a cylindrical shape with a uniform diameter D and length l ($=l_B = l_T$). The incident angle of the light beam is θ. As a comparison, we also calculate a similar three layer system without layer 2 in Figure 5 to simulate the optical properties of air−single nanorod arrays−glass system. The detailed derivations of the calculation equations are shown in Appendix A.

To calculate the optical properties, we set the following parameters as constants: the volume fraction of silver $f = 0.4$, the tilting angles $\beta_T = 73°$ and $\beta_B = -73°$, the diameter $D = 80$ nm, the incident angle of light beam $\theta = 0°$, and the layer thickness $d_T = d_B =$ 120, 160, 200, and 240 nm, which correspond to the nanorod lengths of 410, 550, 680, and 820 nm. As mentioned in Appendix A, the aspect ratio is an important parameter in the effective media

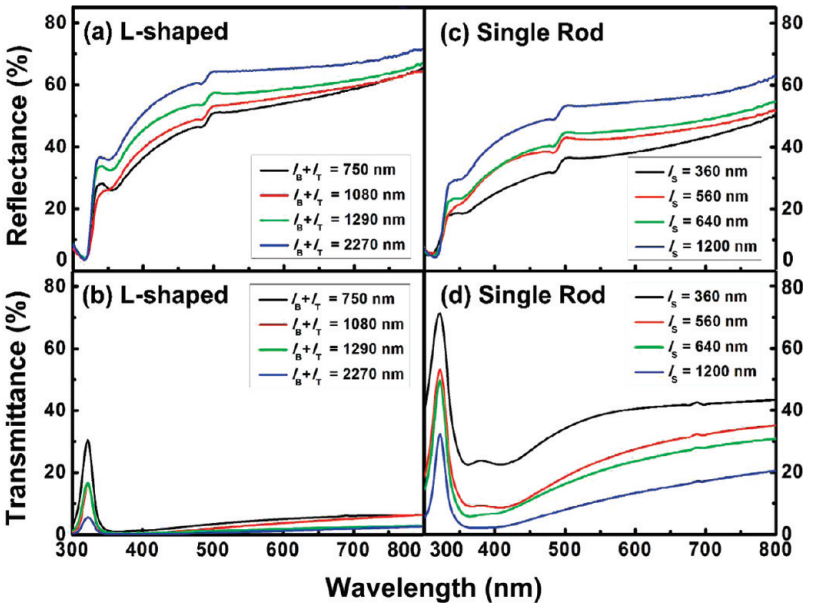

Figure 3. Reflectance and transmittance spectra of L-shaped and single Ag nanorod arrays: (a) reflectance spectra of L-shaped Ag nanorod arrays with total arm length l = 750, 1080, 1290, and 2270 nm; (b) transmittance spectra of L-shaped Ag nanorod arrays with l = 750, 1080, 1290, and 2270 nm; (c) reflectance spectra of single Ag nanorod arrays with l = 360, 560, 640, and 1200 nm; (d) transmittance spectra of single Ag nanorod arrays with l = 360, 560, 640, and 1200 nm.

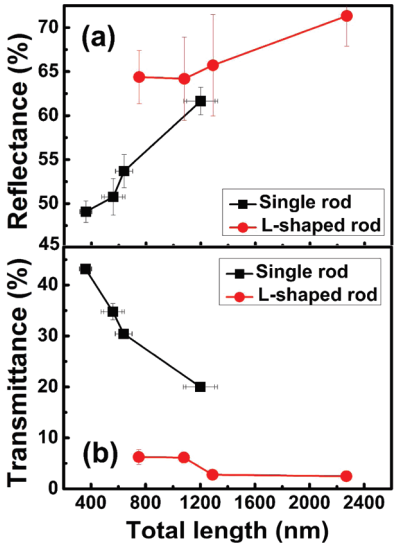

Figure 4. The reflectance and transmittance of L-shaped and single Ag nanorod arrays change as a function of the length of rods with the wavelength of incident light 550 nm: (a) reflectance comparison; (b) transmittance comparison.

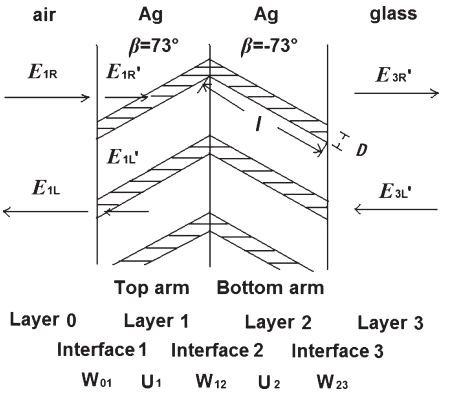

Figure 5. Transfer matrix method of L-shaped Ag nanorod arrays on glass substrate.

theory calculation, and the aspect ratio of silver nanorods is set to be the arm length divided by the diameter 80 nm. The bulk dielectric constant of silver as a function of wavelength is obtained from ref 59. All the calculations were performed using MATLAB 7.

Figure 6 shows the calculated reflectance and transmittance spectra of both L-shaped and single silver nanorod arrays with the different rod length. The trends of the calculated spectra are similar to the experimental ones as shown in Figure 3. They all have nearly constant R and T values in the near-IR region, and the R deceases when λ <450 nm; the T has a broad peak around λ = 400 nm, which is unlike the sharp peak at λ = 320 nm observed in the experiments. The reflectance of the L-shaped Ag nanorod arrays becomes larger when their arms become longer; while the transmittance becomes smaller when their arms become longer. The reflectance and transmittance of the single Ag nanorod arrays follow the same trends as those of the L-shaped Ag nanorod arrays, but the reflectance is smaller than that of the L-shaped Ag nanorod arrays with the same bottom or top arm length, and the transmittance is larger than that of the L-shaped Ag nanorod arrays. All the characterizations of the calculated reflectance and transmittance are consistent qualitatively with those obtained in the experiments. Figure 7 shows the reflectance and transmittance at λ = 550 nm calculated from both the L-shaped and straight nanorod arrays in order to compare their optical properties quantitatively. The general trend is consistent with that obtained experimentally (Figure 4): the reflectance increases while the transmittance decreases as the length of the nanorods increases, for both the L-shaped and straight nanorod arrays. However, the calculated result shows a continuous transition in both R and T from single nanorods to L-shaped nanorods, while

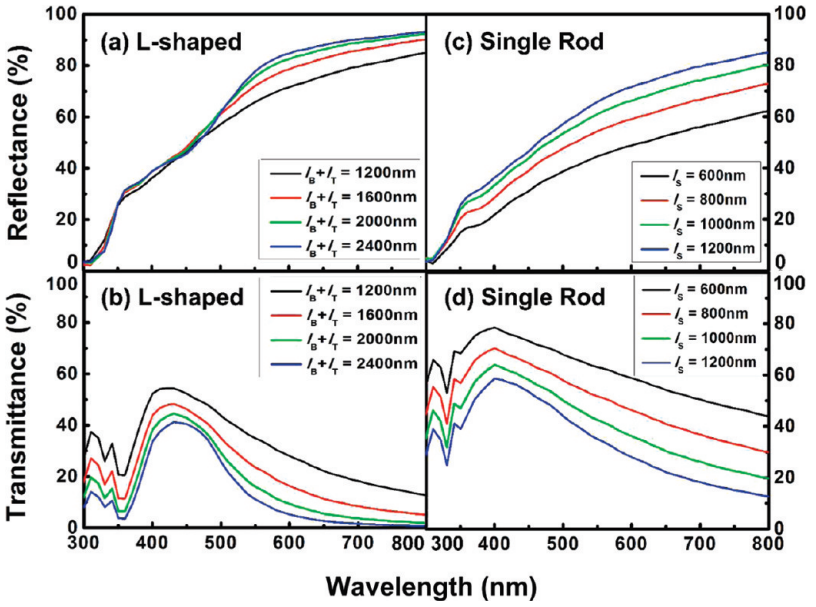

Figure 6. The simulation reflectance and transmittance of L-shaped and single Ag nanorod arrays: (a) reflectance of L-shaped Ag nanorod arrays with total arm lengths 1200, 1600, 2000, and 2400 nm; (b) transmittance of L-shaped Ag nanorod arrays with total arm lengths 1200, 1600, 2000, and 2400 nm; (c) reflectance of single Ag nanorod arrays with rod lengths 600, 800, 1000, and 1200 nm; (d) transmittance of single Ag nanorod arrays with rod lengths 600, 800, 1000, and 1200 nm.

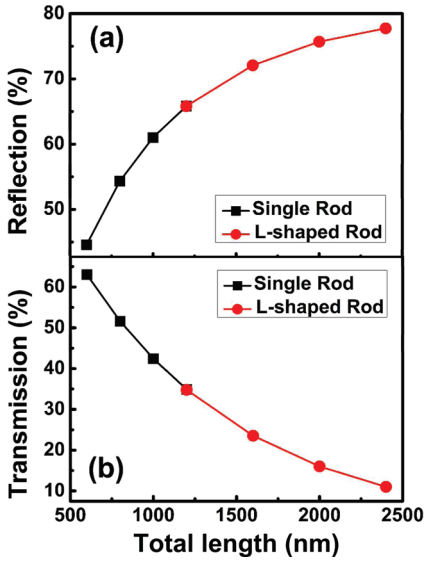

Figure 7. The simulation reflectance and transmittance of L-shaped and single Ag nanorod arrays changes as a function of the length of rods with the wavelength of incident light 550 nm: (a) reflectance comparison; (b) transmittance comparison.

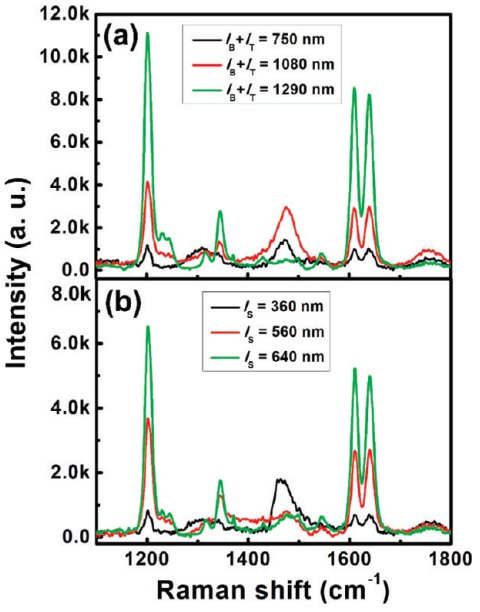

Figure 8. The representative BPE SERS spectra obtained at λ = 785 nm using L-shaped silver nanorod arrays and single silver nanorod arrays as SERS substrates: (a) using L-shaped silver nanorod arrays as SERS substrates; (b) using single silver nanorod arrays as SERS substrates.

experimental data demonstrate discrepancy discontinuity between the data from the L-shaped and those from the straight nanorods. This difference could result from several simple assumptions made in the calculation. For example, both the top and bottom arm layers of the L-shaped Ag nanorods are assumed to have the same volume fraction of silver; both the top and bottom nanorods are assumed to have the same rod diameter, arm length, and tilting angle; and each nanorod is assumed to have a perfect cylindrical shape.

3.4. SERS Characterization. The representative SERS spectra of BPE on the L-shaped and straight silver nanorod arrays are shown in Figure 8. Each spectrum plotted in Figure 8 is an averaged spectrum at least from 15 different sampling spots on the substrates. All the SERS spectra show three characteristic peaks of BPE: $\Delta\nu$ = 1639, 1610, and 1200 cm^{-1}, which can be assigned to the C═C stretching mode, aromatic ring stretching mode, and in-plane ring mode, respectively.[55] The relative peak intensities shown in Figure 8 are very different from those reported in previous studies.[56,57] This is due to the calibration of the sensitivity of the detector in our Raman instrument (see Supporting Information for

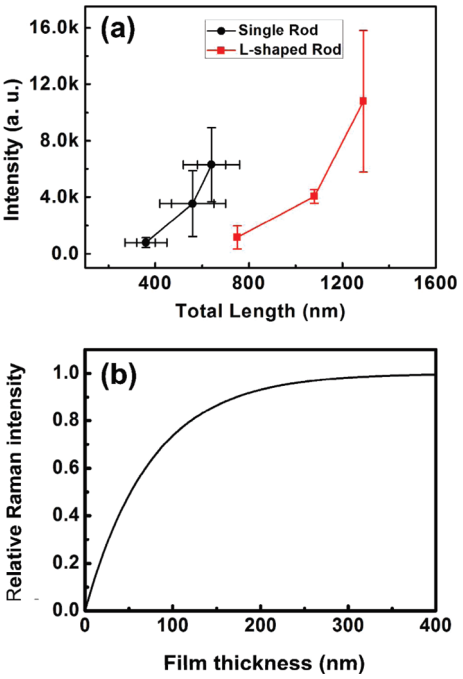

Figure 9. SERS intensity vs rod length and film thickness: (a) SERS intensity vs total length of single rods and L-shaped rods; (b) the calculated relative Raman intensity (eq 6 or eq 7) as a function of film thickness.

the details), and will not affect the relative intensity comparison below. Since for all the SERS measurements the volume and concentration of BPE solution dispensed on the substrates are the same, the droplet spreading areas are similar, and the measurement instrument is the same, one can perform a direct comparison of SERS enhancement using the spectral peaks shown in Figure 8. Figure 9a shows the Raman peak intensities at 1200 cm^{-1} of the straight and L-shaped rod arrays as functions of the total rod length, respectively. For the L-shaped silver nanorod arrays, the Raman intensity increases when the total arm length increases from l = 750 nm to l = 1080 nm to l = 1290 nm. Comparison between single silver nanorod arrays shows the same trend, the Raman intensity with lengths of l = 360, 560, and 640 nm becomes stronger when rod length increases. The enhanced factor of the L-shaped nanorod arrays with a total arm length of l = 750 nm (whose bottom and top arm lengths are both approximately 375 nm) is higher than that of the single nanorod arrays with l = 360 nm. In general, the enhanced factor of the L-shaped nanorods with a total arm lengh l is higher than that of the single nanorods with a total arm length $l/2$. However, the experimental results show that the SERS intensity of the L-shaped nanorod arrays is lower than that of the single nanorods with the same total length.

3.5. The Relationship of SERS and Optical Properties. Previously we predicted that the SERS intensity of the L-shaped nanorod arrays should be higher than that of the single nanorod arrays with the same total length, since the L-shaped nanorods should have more "hot spots". However, our experimental results show that the SERS properties of the L-shaped nanorod arrays with a total arm length of l are quite different from those of the single nanorod arrays with an arm length of $l/2$ but are similar to those of the single nanorod arrays with a total arm length l. A possible explanation for this phenomenon is that the top arm layer of the L-shaped silver nanorod arrays contributes to the most SERS enhancement. The attenuation of the excitation light intensity along the depth of the nanorod arrays and the amount of molecules absorbed on the nanorods at different rod depth are two possible reasons. On the basis of this argument, we propose the following phenomenological model: We believe that the main SERS mechanism for the L-shaped Ag nanorod array substrates is electromagnetic enhancement, and everywhere along the nanorods contributes the same SERS intensity when the intensity of excitation light and the amount of absorbed molecules are the same; i.e., the enhancement factor is the same. However, due to the layer absorbance of Ag nanorods, the excitation light intensity decreases when it penetrates deeper into the nanorod arrays and the SERS contribution along nanorods will be reduced with the depth.[58] Thus, in order to obtain the total SERS intensity, one has to account for all the SERS intensity contributions from different depths of the nanorods. To be simplified, we do not consider the polarization effect of the excitation laser or backward reflectance and we assume that the BPE molecules are distributed uniformly on the surfaces of the Ag nanorods. In order to calculate the total SERS intensity, one needs to find out the incident excitation laser intensity at an arbitrary depth of the nanorods, and after the Raman molecules are excited, the SERS intensity will be attenuated while it passes through the penetration layer according to the backward detection geometry.[60]

For the L-shaped nanorods with the bottom layer thickness d_B and top layer thickness d_T, the excitation laser intensity inside the rod can be expressed in two parts, between interfaces 1 and 2 and between interfaces 2 and 3. Considering a small nanorod section Δd_x at a depth of d_x, the excitation laser intensity between interfaces 1 and 2 is

$$I_{d_x} = I_0 T_1 e^{-\alpha_1 d_x} \quad (1)$$

and between interfaces 2 and 3

$$I_{d_x} = I_0 T_1 T_2 e^{-\alpha_1 d_T - \alpha_2 (d_x - d_T)} \quad (2)$$

where I_0 is the incident intensity

$$T_1 = \left|\frac{E_{1R}}{E_{1R'}}\right|^2, \quad T_2 = \left|\frac{E_{2R}}{E_{2R'}}\right|^2$$

and the E-field of incident light at interface 1 is E_{1R}, and the E-field incident at interface 2 is E_{2R}, and comes out from interface 2 is E_{2R}', and α_1 and α_2 are the absorbance coefficient at these two regions. The SERS intensity contribution from such a small section Δd_x can be expressed as

$$\Delta I_{SERS} = I_0 \sigma G T_1^2 e^{-2\alpha_1 d_x} \Delta d_x \quad (3)$$

between interfaces 1 and 2 and

$$\Delta I_{SERS} = I_0 \sigma G T_1^2 T_2^2 e^{-2\alpha_1 d_T - 2\alpha_2 (d_x - d_T)} \Delta d_x \quad (4)$$

between interfaces 2 and 3, where G is the SERS enhancement factor, and σ is the linear density of BPE on nanorods. The total SERS intensity of L-shaped nanorods is

$$I_{SERS} = \int_0^{d_T} I_0 \sigma G T_1^2 e^{-2\alpha_1 d_x} \, dd_x + \int_{d_T}^{d_T + d_B} I_0 \sigma G T_1^2 T_2^2 e^{-2\alpha_1 d_T - 2\alpha_2 (d_x - d_T)} \, dd_x \quad (5)$$

The result shown in Figure 4 suggests that T_2 is much smaller than T_1, i.e.,

$$\int_0^{d_T} I_0\sigma G{T_1}^2 e^{-2\alpha_1 d_x}\, dd_x \gg \int_{d_T}^{d_T+d_B} I_0\sigma G{T_1}^2{T_2}^2 e^{-2\alpha_1 d_T - 2\alpha_2(d_x - d_T)}\, dd_x$$

Therefore

$$I_{SERS} = \int_0^{d_T} I_0\sigma G{T_1}^2 e^{-2\alpha_1 d_x}\, dd_x + \int_{d_T}^{d_T+d_B} I_0\sigma G{T_1}^2{T_2}^2 e^{-2\alpha_1 d_T - 2\alpha_2(d_x - d_T)}\, dd_x \approx \int_0^{d_T} I_0\sigma G{T_1}^2 e^{-2\alpha_1 d_x}\, dd_x \quad (6)$$

For single nanrods with total thickness of d_T, since there is only one layer, the SERS intensity can be expressed as,

$$I_{SERS} = \int_0^{d_T} I_0\sigma G{T_1}^2 e^{-2\alpha_1 d_x}\, dd_x \quad (7)$$

In fact, the expression for eq 6 and eq 7 is similar, and the calculation result from these two equatios is shown in Figure 9b. This result suggests that the SERS intensity of single nanorod arrays with total thickness equal to the top layer thickness of L-shaped ones is similar to the SERS intensity of L-shaped nanorod arrays, which matches the experimental results. With the increase of the nanorod thickness, the SERS intensity increases. This is consistent with the SERS intensity of both the L-shaped and straight nanorods at small nanorod thickness. From eq 6 one sees that the SERS from the bottom arm layer of L-shaped nanorods contributes a very small part of the total SERS signal. So, SERS intensity of L-shaped rods is higher than that of single rods with the same rod length as their arm length; SERS intensity of L-shaped rods is much lower than that of single rods with twice rod length as their arm length at the range when intensity increases.

4. CONCLUSIONS

In conclusion, the OAD method is used to fabricate L-shaped Ag nanorod arrays by change of the vapor incident direction during deposition. The optical properties, including reflectance and transmittance spectra of L-shaped Ag nanorod arrays, were experimentally measured and theoretically calculated, and compared to those of single Ag nanorod arrays. For both L-shaped Ag nanorod arrays and single Ag nanorod arrays, the reflectance increases as rod length increases, while transmittance decreases. The reflectance behavior of the L-shaped nanorod arrays versus rod length is similar to that of the single nanorod arrays with rod length is equal to the total L-shaped nanorod length of two arms. Calculation based on the transfer matrix method shows similar results as those measured experimentally. The SERS properties of L-shaped Ag nanorod arrays and single Ag nanorod arrays have been explored using BPE as the Raman probe. The SERS enhanced factor of both kinds of nanorod arrays increase when the rod length increases from 350 to 650 nm. The SERS properties of L-shaped nanorod arrays are quite different from those of single nanorod arrays with the same arm length, but are similar to those of single nanorod arrays with the same total rod length. We believe that this behavior can be explained by the layer absorbance during the excitation and SERS signal propagating through the thick nanorod layer.

APPENDIX A: EFFECTIVE MEDIUM THEORY ON THE OPTICAL PROPERTIES OF L-SHAPED AG NANORODS

The L-shaped nanorod layer can be treated as two anisotropic layers due to the tilting nature, and we consider a four-layer model with the structure of air layer (layer 0), top arm of L-shaped nanorod layer (layer 1), bottom arm of L-shaped nanorod layer (layer 2), and glass layer (layer 3), as shown in Figure 4. We define the top Ag NR layer (layer 1) as an effective medium layer with a thickness d_T which is composed of the Ag nanorods and air between tilted with angle β_T with respect to surface normal and the bottom Ag layer (layer 2) as another effective medium layer with a thickness of d_B which is also composed of the nanorods and air with a tilting angle of $-\beta_B$. To be simplified, we assume all the Ag NRs have a cylindrical shape with a uniform diameter D and length l. The incident angle of light beam is θ. As a comparison, we also calculate a similar three layer system without layer 2 in the Figure 4 to simulate the optical properties of air−single nanorod arrays−glass system.

In layer 1 and layer 2 silver nanorods are porous and anisotropic and we use an anisotropic effective medium theory to calculate effective optical properties.[41,42] The incidence plane is defined by the incident beam and interface normal. It is parallel to the nanorod tilting plane and is defined as the $x-z$ plane. The dielectric constant for these two layers is described by a tensor. The components of the dielectric tensor $\vec{\varepsilon}_1$ of layer 1 and $\vec{\varepsilon}_2$ of layer 2 in the coordinate system xyz are all nonzero. For simplifying the representation of $\vec{\varepsilon}_1$ and $\vec{\varepsilon}_2$, we rotate the xyz coordinates by the angle of β around the y axis and make each axis of the new $x'y'z'$ coordinates parallel to one of the principal axes of the nanorods.[26] We define the dielectric constants in three principal axes $\varepsilon_{x'}$, $\varepsilon_{y'}$, and $\varepsilon_{z'}$, which depend on the material and the shape of nanorods. For each arm of L-shaped nanorod and single nanorod, the dielectric constant tensor $\vec{\varepsilon}_1$ is

$$\vec{\varepsilon_i} = \begin{pmatrix} \varepsilon_{x'} & 0 & \\ 0 & \varepsilon_{y'} & 0 \\ & 0 & \varepsilon_{z'} \end{pmatrix}, \quad \text{where } \varepsilon_{x'} = \varepsilon_{y'},\ i = 1, 2 \quad (1A)$$

The dielectric constant tensor $\vec{E}^i$ in the xyz coordinates is

$$\vec{E}^i = \begin{pmatrix} \varepsilon^i_{xx} & \varepsilon^i_{xy} & \varepsilon^i_{xz} \\ \varepsilon^i_{yx} & \varepsilon^i_{yy} & \varepsilon^i_{yz} \\ \varepsilon^i_{zx} & \varepsilon^i_{zy} & \varepsilon^i_{zz} \end{pmatrix} = \begin{pmatrix} \varepsilon_{x'}\cos^2\beta + \varepsilon_{z'}\sin^2\beta & 0 & -\varepsilon_{x'}\sin\beta\cos\beta + \varepsilon_{z'}\sin\beta\cos\beta \\ 0 & \varepsilon_{y'} & 0 \\ -\varepsilon_{x'}\sin\beta\cos\beta + \varepsilon_{z'}\sin\beta\cos\beta & 0 & \varepsilon_{x'}\sin^2\beta + \varepsilon_{z'}\cos^2\beta \end{pmatrix} \quad (2A)$$

1. Effective Medium Theory. Layer 1 and layer 2 can be treated as an effective medium layer composed by metal nanorods and air. The theoretical formulations developed by Maxwell−Garnett (MG) and Bruggeman (BR) are well known

and widely used. The BR theory presumes structural equivalence between two constituents, while the MG theory applies to particles separated in a host. In our study, air is separated in continual porous metal structures; thus the MG theory is used, which yields in the $x'y'z'$ coordinates system:

$$\frac{\varepsilon_i - \varepsilon_m}{\varepsilon_m + L_i(\varepsilon_i - \varepsilon_m)} = (1 - f_m)\frac{\varepsilon_a - \varepsilon_m}{\varepsilon_m + L_i(\varepsilon_a - \varepsilon_m)} \quad (3A)$$

$$i = x', y', z', \quad L_{x'} + L_{y'} + L_{z'} = 1$$

$$\Rightarrow \varepsilon_i = \frac{\varepsilon_m + (\varepsilon_a - \varepsilon_m)(f_m L_i + 1 - fm)}{\varepsilon_m + (\varepsilon_a - \varepsilon_m)(f_m L_i)} \quad (4A)$$

where ε_m and ε_a are the dielectric constants of metal and air, respectively, f_m is the volume fraction of metal, and L_i is the depolarization factor in the $x'y'z'$ coordinate system. When the structure considered is of the prolate spheroid shape

$$L_{z'} = \frac{1 - e^2}{e^2}\left[\frac{1}{2e}\ln\left(\frac{1 + e}{1 - e}\right) - 1\right] \quad (5A)$$

$$e = \sqrt{1 - r^2}, \quad L_{x'} = L_{y'} = \frac{1}{2}(1 - L_{z'})$$

where r presents aspect ratio of the spheriod, $r = D/l$.

2. Transfer Matrix. As plotting in Figure 4, we define that E_{iR} presents electric field amplitudes of the light at interface i (interface between the layer $i - 1$ and the layer i) from layer $i - 1$ to layer i, and still in the layer $i - 1$; E_{iR}' presents electric field amplitudes from layer $i - 1$ to layer i, and already in the layer i; E_{iL} and E_{iL}' present electric field amplitudes of the light from layer i to layer $i - 1$, as shown Figure 4. The reflectance R and transmittance T of the multilayer system can be calculated from r and t

$$r = \frac{E_{1L}}{E_{1R}}, \quad t = \frac{E_{3R}'}{E_{1R}} \text{ when } E_{3L}' = 0 \quad (6A)$$

At every interface

$$r_{iR} = \frac{E_{iL}}{E_{iR}}, \quad t_{iR} = \frac{E_{iR}'}{E_{iR}}, \quad r_{iL} = \frac{E_{iR}'}{E_{iL}'}, \quad t_{iL} = \frac{E_{iL}}{E_{iL}'}$$
$$\text{where } i = 1, 2, 3 \quad (7A)$$

where $i = 1, 2, 3$ and r_{iR} and t_{iR} present reflectance and transmittance coefficients when light goes to the layer i from layer $i - 1$ at the interface i, respectively; r_{iL} and t_{iL} present reflectance and transmittance coefficients when light goes to the layer $i - 1$ from the layer i at the interface i, respectively.

According to standard Fresnel formula if the medium is isotropic, for s waves

$$r_{iR} = \frac{n_i \cos\theta_{i-1} - n_i \cos\theta_i}{n_i \cos\theta_{i-1} + n_i \cos\theta_i},$$
$$t_{iR} = \frac{2n_{i-1} \cos\theta_{i-1}}{n_{i-1} \cos\theta_{i-1} + n_i \cos\theta_i},$$
$$r_{iL} = \frac{n_i \cos\theta_i - n_{i-1} \cos\theta_{i-1}}{n_{i-1} \cos\theta_{i-1} + n_{i-1} \cos\theta_i},$$
$$t_{iL} = \frac{2n_i \cos\theta_i}{n_{i-1} \cos\theta_{i-1} + n_i \cos\theta_i},$$
$$\text{where } i = 1, 2, 3 \quad (8A)$$

For p waves

$$r_{iR} = \frac{n_i \cos\theta_{i-1} - n_{i-1} \cos\theta_i}{n_i \cos\theta_{i-1} + n_{i-1} \cos\theta_i}, \quad t_{iR} = \frac{2n_{i-1} \cos\theta_{i-1}}{n_i \cos\theta_{i-1} + n_{i-1} \cos\theta_i},$$
$$r_{iL} = \frac{n_{i-1} \cos\theta_i - n_i \cos\theta_{i-1}}{n_i \cos\theta_{i-1} + n_{i-1} \cos\theta_i}, \quad t_{iL} = \frac{2n_i \cos\theta_i}{n_i \cos\theta_{i-1} + n_{i-1} \cos\theta_i},$$
$$\text{where } i = 1, 2, 3 \quad (9A)$$

When there are anisotropic layers in the multilayer optic system, we need to adjust the formula to consider the anisotropic dielectric constant of the medium. Here we use the surface admittance Y and surface impedance Z, which are defined in terms of the field components parallel to the interface. For s waves

$$r_{iR} = \frac{Y_{i-1} - Y_i}{Y_{i-1} + Y_i}, \quad t_{iR} = \frac{2Y_{i-1}}{Y_{i-1} + Y_i}, \quad r_{iL} = \frac{Y_i - Y_{i-1}}{Y_{i-1} + Y_i},$$
$$t_{iL} = \frac{2Y_i}{Y_{i-1} + Y_i}, \text{ where } i = 1, 2, 3 \quad (10A)$$

$$Y_0 = n_0 \cos\theta$$
$$Y_i = \sqrt{\varepsilon_{y'} - \varepsilon_{air} \sin^2\theta}, \text{ where } i = 1, 2 \quad (11A)$$
$$Y_3 = \sqrt{\varepsilon_{glass} - \varepsilon_{air} \sin^2\theta}$$

For p waves

$$r_{iR} = \frac{Z_{i-1} - Z_i}{Z_{i-1} + Z_i}, \quad t_{iR} = \frac{2Z_{i-1}}{Z_{i-1} + Z_i}, \quad r_{iL} = \frac{Z_i - Z_{i-1}}{Z_{i-1} + Z_i},$$
$$t_{iL} = \frac{2Z_i}{Z_{i-1} + Z_i}, \quad \text{where } i = 1, 2, 3 \quad (12A)$$

$$Z_0 = \cos\theta / n_0$$
$$Z_i = \sqrt{\frac{\varepsilon_{zz} - \varepsilon_{air} \sin^2\theta}{\varepsilon_{x'}\varepsilon_{y'}}}, \text{ where } i = 1, 2 \quad (13A)$$
$$Z_3 = \frac{1}{\varepsilon_{glass}}\sqrt{\varepsilon_{glass} - \varepsilon_{air} \sin^2\theta}$$

After calculating r_{iR}, t_{iR}, r_{iL}, and t_{iL}, we can derive how field amplitudes change at each interface. The amplitudes in the layer i fields are related to those in the layer $i - 1$ fields by

$$E_{iL} = r_{iR}E_{iR} + t_{iL}E_{iL}'$$
$$E_{iR}' = t_{iR}E_{iR} + r_{iL}E_{iL}' \quad (14A)$$

Then the field amplitudes at each side of the multilayer can be related by a 2×2 matrix $W_{(i-1)i}$, derived from the above equations, which is called the refractive matrix.

$$\begin{bmatrix} E_{iR} \\ E_{iL} \end{bmatrix} = W_{(i-1)i}\begin{bmatrix} E_{iR}' \\ E_{iL}' \end{bmatrix} \quad (15A)$$

where

$$W_{(i-1)i} = \frac{1}{t_{iR}}\begin{bmatrix} 1 & -r_{iL} \\ t_{iR} & t_{iR}t_{iL} - r_{iR}r_{iL} \end{bmatrix}$$

We use matrix U_i to describe the effect of light propagation through the homogeneous layer i alone, which is called the phase matrix.

$$\begin{bmatrix} E_{iR}' \\ E_{iL}' \end{bmatrix} = U_i\begin{bmatrix} E_{(i+1)R} \\ E_{(i+1)L} \end{bmatrix} \quad (16A)$$

where

$$U_i = \begin{bmatrix} \exp(i\varphi_i) & 0 \\ 0 & \exp(-i\varphi_i) \end{bmatrix}$$

φ_i is phase shift in layer i because of the optical path difference, if the thickness of the layer is on the order of the wavelength of incident radiation.

To calculate the phase propagation in the anisotropic medium, we introduce the wave vector $k = (k_x, k_z) = k_0(N + iK)$ for defining wave direction, refractive index, and phase shift across the film.

$$k_z{}^s = k_0(N_z{}^s + iK_z{}^s) = k_0\sqrt{\varepsilon_{y'} - \varepsilon_i \sin^2\theta}$$
$$k_{z\pm}{}^p = k_0(N_z{}^p + iK_z{}^p) = k_0\left(\frac{\varepsilon_{xz}\sin\theta \pm \varepsilon_{x'}\varepsilon_{z'}Z_i}{\varepsilon_{zz}}\right) \quad (17A)$$

where $i = 1, 2$. Then, for s waves

$$U_{is} = \begin{bmatrix} \exp(ik_z{}^s d_i) & 0 \\ 0 & \exp(-ik_z{}^s d_i) \end{bmatrix} \quad (18A)$$

For p waves

$$U_{ip} = \begin{bmatrix} \exp(ik_{z+}{}^p d_i) & 0 \\ 0 & \exp(-ik_{z-}{}^p d_i) \end{bmatrix} \quad (19A)$$

where $i = 1, 2$. When the light propagates through an $i + 1$ layers optical system, the field amplitudes change at interfaces i and $i - 1$ homogeneous layers. Thus, one can achieve the field amplitudes at the end from the origin field amplitudes by i refractive matrix and $i - 1$ phase matrix.

$$\begin{bmatrix} E_{1R} \\ E_{1L} \end{bmatrix} = W_{0i}\begin{bmatrix} E_{iR}{}' \\ E_{iL}{}' \end{bmatrix}$$
$$= W_{01}U_1W_{12}U_2\ldots U_{i-1}W_{(i-1)i}\begin{bmatrix} E_{iR}{}' \\ E_{iL}{}' \end{bmatrix} \quad (20A)$$

Define

$$W_{0i} = \begin{bmatrix} s_{11} & s_{12} \\ s_{21} & s_{22} \end{bmatrix}$$

As a result

$$r_{system} = \frac{s_{21}}{s_{11}}, \quad t_{system} = \frac{1}{s_{11}} \quad (21A)$$

and

$$R_{system} = |r_{system}|^2, \quad T_{system} = |t_{system}|^2 \quad (22A)$$

■ ASSOCIATED CONTENT

Supporting Information. Figures showing the SERS spectra of BPE measured with 785 and 532 excitation. This material is available free of charge via the Internet at http://pubs.acs.org.

■ AUTHOR INFORMATION

Corresponding Author
*E-mail: zhaoy@physast.uga.edu.

■ ACKNOWLEDGMENT

The authors Q. Zhou and Z.J. Zhang are grateful to the financial support by China Scholarship Council and the National Natural Science Foundation of China (50931002). Q. Zhou, J. Abell, Y.P. He, and Y.P. Zhao thank the support from National Science Foundation (Grant No. ECCS-0701787 and ECCS-1029609). The authors also thank Mr. Chunyuan Song for helping in SERS measurement using the Bruker system.

■ REFERENCES

(1) Michaels, A. M.; Jiang, J.; Brus, L. *J. Phys. Chem. B* **2000**, *104*, 11965.
(2) Huh, Y. S.; Chung, A. J.; Erickson, D. *Microfluid. Nanofluid.* **2009**, *6*, 285.
(3) Han, X. X.; Zhao, B.; Ozaki, Y. *Anal. Bioanal. Chem.* **2009**, *394*, 1719.
(4) Lin, X. M.; Cui, Y.; Xu, Y. H.; Ren, B.; Tian, Z. Q. *Anal. Bioanal. Chem.* **2009**, *394*, 1729.
(5) Kneipp, K.; Kneipp, H.; Itzkan, I.; Dasari, R. R.; Feld, M. S. *Chem. Rev.* **1999**, *99*, 2957.
(6) Constantino, C.; Lemma, T.; Antunes, P. A.; Aroca, R. *Anal. Chem.* **2001**, *73*, 3674.
(7) Doering, W. E.; Nie, S. M. *J. Phys. Chem. B* **2002**, *106*, 311.
(8) Nie, S. M.; Emery, S. R. *Science* **1997**, *275*, 1102.
(9) Kneipp, K.; Wang, Y.; Kneipp, H.; Perelman, L. T.; Itzkan, I.; Dasari, R.; Feld, M. S. *Phys. Rev. Lett.* **1997**, *78*, 1667.
(10) Moskovits, M. *Rev. Mod. Phys.* **1985**, *57*, 783.
(11) Campion, A.; Kambhampati, P. *Chem. Soc. Rev.* **1998**, *27*, 241.
(12) Freeman, R. G.; Bright, R. M.; Hommer, M. B.; Natan, M. J. *J. Raman Spectrosc.* **1999**, *30*, 733.
(13) Xu, H. X.; Aizpurua, J.; Kall, M.; Apell, P. *Phys. Rev. E* **2000**, *62*, 4318.
(14) Lu, Y.; Liu, G. L.; Lee, L. P. *Nano Lett.* **2005**, *5*, 5.
(15) McFarland, A. D.; Young, M. A.; Dieringer, J. A.; Van Duyne, R. P. *J. Phys. Chem. B* **2005**, *109*, 11279.
(16) Qin, L. D.; Zou, S. L.; Xue, C.; Atkinson, A.; Schatz, G. C.; Mirkin, C. A. *Proc. Natl. Acad. Sci. U.S.A.* **2006**, *103*, 13300.
(17) Liu, Y. J.; Zhang, Z. Y.; Zhao, Q.; Dluhy, R. A.; Zhao, Y. P. *J. Phys. Chem. C* **2009**, *113*, 9664.
(18) Zhang, Z. Y.; Zhao, Y. P. *J. Appl. Phys.* **2007**, *102*.
(19) Zhang, Z. Y.; Zhao, Y. P. *Appl. Phys. Lett.* **2006**, *89*.
(20) Sun, X. Z.; Lin, L. H.; Li, Z. C.; Zhang, Z. J.; Feng, J. Y. *Mater. Lett.* **2009**, *63*, 2306.
(21) Huang, Z. L.; Meng, G. W.; Huang, Q.; Yang, Y. J.; Zhu, C. H.; Tang, C. L. *Adv. Mater.* **2010**, *22*, 4136.
(22) Liu, Y. J.; Zhang, Z. Y.; Zhao, Q.; Dluhy, R. A.; Zhao, Y. P. *Appl. Phys. Lett.* **2009**, *94*.
(23) Chaney, S. B.; Shanmukh, S.; Dluhy, R. A.; Zhao, Y. P. *Appl. Phys. Lett.* **2005**, *87*.
(24) Tripp, R. A.; Dluhy, R. A.; Zhao, Y. P. *Nano Today* **2008**, *3*, 31.
(25) Zhou, Q.; Li, Z. C.; Yang, Y.; Zhang, Z. J. *J. Phys. D: Appl. Phys.* **2008**, *41*.
(26) Driskell, J. D.; Shanmukh, S.; Liu, Y.; Chaney, S. B.; Tang, X. J.; Zhao, Y. P.; Dluhy, R. A. *J. Phys. Chem. C* **2008**, *112*, 895.
(27) Zhou, Q.; Yang, Y.; Ni, J.; Li, Z. C.; Zhang, Z. J. *Phys. E (Amsterdam, Neth.)* **2010**, *42*, 1717.
(28) Zhou, Q.; Yang, Y.; Ni, J. E.; Li, Z. C.; Zhang, Z. J. *Nano Res.* **2010**, *3*, 423.
(29) Zhou, Q.; Liu, Y. J.; He, Y. P.; Zhang, Z. J.; Zhao, Y. P. *Appl. Phys. Lett.* **2010**, *97*.

(30) Messier, R.; Venugopal, V. C.; Sunal, P. D. *J. Vac. Sci. Technol., A* **2000**, *18*, 1538.
(31) Kennedy, S. R.; Brett, M. J.; Toader, O.; John, S. *Nano Lett.* **2002**, *2*, 59.
(32) Kesapragada, S. V.; Victor, P.; Nalamasu, O.; Gall, D. *Nano Lett.* **2006**, *6*, 854.
(33) Motohiro, T.; TAGA, Y. *Appl. Opt.* **1989**, *28*, 2466.
(34) Robbie, K.; Brett, M. J.; Lakhtakia, A. *Nature* **1996**, *384*, 616.
(35) Robbie, K.; Brett, M. J. *J. Vac. Sci. Technol., A* **1997**, *15*, 1460.
(36) Robbie, K.; Sit, J. C.; Brett, M. J. *J. Vac. Sci. Technol., B* **1998**, *16*, 1115.
(37) Messier, R.; Lakhtakia, A. *Mater. Res. Innovations* **1999**, *2*, 217.
(38) Zhao, Y. P.; Ye, D. X.; Wang, G. C.; Lu, T. M. *Nano Lett.* **2002**, 351.
(39) Zhao, Y. P.; Ye, D. X.; Wang, P. I.; Wang, G. C.; Lu, T. M. *Int. J. Nanosci.* **2002**, 87.
(40) He, Y. P.; Fu, J. X.; Zhang, Y.; Zhao, Y. P.; Zhang, L.; Xia, A.; Cai, J. *Small* **2007**, 153.
(41) Shanmukh, S.; Jones, L.; Driskell, J.; Zhao, Y. P.; Dluhy, R.; Tripp, R. A. *Nano Lett.* **2006**, *6*, 2630.
(42) Shanmukh, S.; Jones, L.; Zhao, Y. P.; Driskell, J. D.; Tripp, R. A.; Dluhy, R. A. *Anal. Bioanal. Chem.* **2008**, *390*, 1551.
(43) Driskell, J. D.; Zhu, Y.; Kirkwood, C. D.; Zhao, Y. P.; Dluhy, R. A.; Tripp, R. A. *PLoS One* **2010**, *5*, DOI: 10.1371/journal.pone.0010222.
(44) Hennigan, S. L.; Driskell, J. D.; Dluhy, R. A.; Zhao, Y. P.; Tripp, R. A.; Waites, K. B.; Krause, D. C. *PLoS One* **2010**, *5*, DOI: 10.1371/journal.pone.0013633.
(45) Driskell, J. D.; Seto, A. G.; Jones, L. P.; Jokela, S.; Dluhy, R. A.; Zhao, Y. P.; Tripp, R. A. *Biosens. Bioelectron.* **2008**, *24*, 917.
(46) Driskell, J. D.; Primera-Pedrozo, O. M.; Dluhy, R. A.; Zhao, Y. P.; Tripp, R. A. *Appl. Spectrosc.* **2009**, *63*, 1107.
(47) Leverette, C. L.; Villa-Aleman, E.; Jokela, S.; Zhang, Z. Y.; Liu, Y. J.; Zhao, Y. P.; Smith, S. A. *Vib. Spectrosc.* **2009**, *50*, 143.
(48) Du, X. B.; Chu, H. Y.; Huang, Y. W.; Zhao, Y. P. *Appl. Spectrosc.* **2010**, *64*, 781.
(49) Smith, G. B. *Appl. Opt.* **1990**, *29*, 3685.
(50) Mitsas, C. L.; SIAPKAS, D. I. *Appl. Opt.* **1995**, *34*, 1678.
(51) Monzon, J. J.; Sanchez-Soto, L. L. *J. Opt. Soc. Am. A* **1999**, *16*, 2013.
(52) Katsidis, C. C.; Siapkas, D. I. *Appl. Opt.* **2002**, *41*, 3978.
(53) Postava, K.; Yamaguchi, T.; Kantor, R. *Appl. Opt.* **2002**, *41*, 2521.
(54) Fu, J. X.; Park, B.; Zhao, Y. P. *Appl. Opt.* **2009**, *48*, 4637.
(55) Yang, W. H.; Hulteen, J.; Schatz, G. C.; VanDuyne, R. P. *J. Chem. Phys.* **1996**, *104*, 4313.
(56) Hulteen, J. C.; Treichel, D. A.; Smith, M. T.; Duval, M. L.; Jensen, T. R.; Van Duyne, R. P. *J. Phys. Chem. B* **1999**, *103*, 3854.
(57) Maxwell, D. J.; Emory, S. R.; Nie, S. *Chem. Mater.* **2001**, *13*, 1082.
(58) Zhang, Z. Y.; Liu, Y. J.; Zhao, Q.; Zhao, Y. P. *Appl. Phys. Lett.* **2009**, *94*.
(59) Palik, E. D. *Handbook of Optical Constants of Solids*; Academic Press: New York, 1985.
(60) Zhou, Q.; He, Y.-P.; Abell, J.; Zhang, Z.-J.; Zhao, Y.-P. *Chem Commun.* **2011**, *47*, 4466–4468.